Cement and Concrete Research 42 (2012) 1066–1071

Contents lists available at SciVerse ScienceDirect

Cement and Concrete Research

journal homepage: http://ees.elsevier.com/CEMCON/default.asp

Tailoring engineered cementitious composites for impact resistance

En-Hua Yang [a], Victor C. Li [b,*]

[a] Civil and Environmental Engineering, Nanyang Technological University, Singapore 639798, Singapore
[b] Civil and Environmental Engineering, University of Michigan, Ann Arbor, MI 48109, USA

ARTICLE INFO

Article history:
Received 6 December 2010
Accepted 19 April 2012

Keywords:
Engineered cementitious composites (ECC)
Micromechanics (C)
Strain-rate effect (C)
Fiber reinforcement (E)
Tensile properties (C)

ABSTRACT

This paper presents results of deliberate tailoring of engineered cementitious composites (ECC) for impact resistance. Microstructure control involving fiber, matrix and fiber/matrix interface was based on steady-state dynamic crack growth analyses accounting for rate dependence of composite phases. Uniaxial tensile stress–strain curves of the resulting impact resistant ECC were experimentally determined for strain rates ranging from $10^{-5}\,s^{-1}$ to $10^{-1}\,s^{-1}$. Low speed drop weight tower test on ECC panels and beams was also conducted. Damage characteristics, load and energy dissipation capacities, and response to repeated impacts, were studied.

1. Introduction

Infrastructure can experience a wide variety of dynamic loads. Severe structural damage or even catastrophic failures have occurred in some extreme events. There is a need to design civil infrastructure resilient to seismic, impact, and blast loading to enhance public safety.

Loading in general, and dynamic loading in particular, can generate tensile stresses in reinforced concrete (R/C) structures. Although a compressive stress wave is generated on the loading side of the structure by impact or blast loading (IBL), it reflects as a tensile stress wave after hitting a free boundary on the distal side of the structural element. Fig. 1 shows the numerically simulated stress states [1] at four time instances after a projectile impacted on an object. Tensile stresses (in red) are generated in the impacted material volume at the circumferential edge of the projectile (Fig. 1b and c). The compressive stress on the distal side (Fig. 1c) changes into tension when the elastic wave reflects off the traction-free back-face (Fig. 1d). Under impact loading, tensile stresses in concrete structure cannot be avoided.

The tensile strength of concrete is typically an order of magnitude lower than its compressive strength. In addition, the fracture toughness of concrete, at about 0.01 MPa $\sqrt{m}$, is among the lowest in construction materials. Therefore, the structural capacity is often limited by the tensile properties of the concrete under IBL [2]. It can be expected that structural integrity loss may be more serious when concrete infrastructure experiences IBL instead of quasi-static loading. Apart from loss of structural integrity, high speed spalling debris ejected from the distal side of the structural elements can cause serious injury to personnel behind the structural elements.

While concrete compressive strength improvements over the last three decades have been impressive, currently attaining over 200 MPa, enhancement of tensile ductility has been achieved only in recent years. Ductile concrete with tensile ductility over 2% has become a reality [3], having been put into full-scale infrastructure such as bridges and buildings [4]. Most studies on ductile concrete have focused on static loading. Investigation of the tensile dynamic response of this class of concrete has just begun.

Engineered cementitious composites (ECC), a unique high performance fiber reinforced concrete featuring high ductility and damage tolerance under tensile and shear loading [5], offers a potential material solution to reducing R/C structure vulnerability under IBL. By employing micromechanics-based material optimization principles [6], tensile strain capacity in excess of 5% under quasi-static uniaxial tensile loading can be attained with only 2% fiber content by volume. Fig. 2 shows a typical uniaxial tensile stress–strain curve of ECC that exhibits a 'strain-hardening' behavior after initial 'yielding' similar to that of ductile metals. The tensile strain capacity of ECC is 500–600 times that of normal concrete. The compressive strength of ECC ranges from 40 to 80 MPa depending on mix composition, the high end similar to that of high strength concrete. ECC represents a concrete material combining high ductility and moderate compressive strength.

R/ECC structural members show superior structural load carrying and energy dissipation capacity and extreme high damage tolerance under monotonic and cyclic loading, when compared with normal R/C structures [7]. The significantly enhanced performance of R/ECC structural elements is a direct result of the ultra-ductility of ECC, which suppresses the brittle failure mode, maintains the structural

* Corresponding author. Tel.: +1 734 764 3368; fax: +1 734 764 4292.
E-mail address: vcli@umich.edu (V.C. Li).

0008-8846/$ – see front matter © 2012 Elsevier Ltd. All rights reserved.
doi:10.1016/j.cemconres.2012.04.006

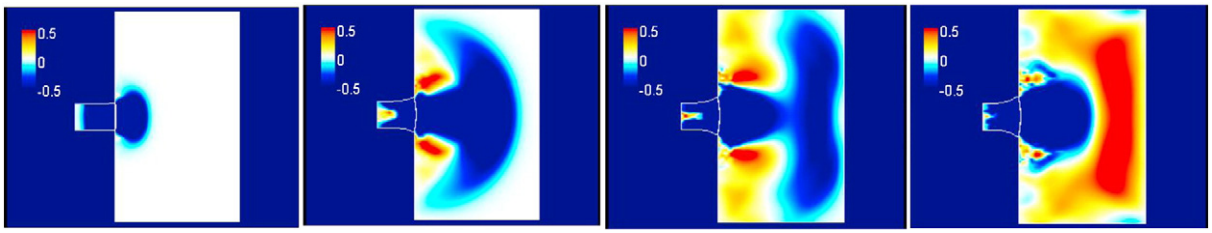

Fig. 1. Numerical simulation of stress state in an elastic–plastic body under impact (after Ref. [1]) at elapse time after impact of (a) 0.2 μs, (b) 0.42 μs, (c) 0.52 μs, and (d) 0.65 μs. Specimen dimension is 2.4 mm × 4.0 mm.

integrity, and promotes the synergistic interaction between steel reinforcement and surrounding ductile ECC material. In addition, the high energy dissipation observed in R/ECC members is a result of the plastic yielding of longer segments of the steel reinforcement in comparison to that in normal R/C members. The engagement of a longer segment of steel yielding is due to the compatible deformation between rebar and ECC in an R/ECC element even when the member undergoes large deformation [8]. It is plausible that this high energy dissipation feature of R/ECC structure may be maintained when subjected to IBL, as long as the deformation compatibility behavior just described could be retained under high rate loading. The success of ECC as a ductile concrete material under IBL depends on its ability to retain tensile ductility at high strain rate, which requires a systematic investigation.

It has been reported that the tensile ductility of ECC M45, a version of ECC with a large database and already applied in engineering practice, reduced from 3.2% to 0.8% as the strain rate increased from quasi-static (10^{-5} s^{-1}) to low speed impact (10^{-1} s^{-1}) as shown in Fig. 3 [9]. It was concluded that the rate dependence in M45 could be attributed to the rate sensitivity in the component phases, which resulted in reduction of ECC multiple cracking and tensile strain-hardening behavior at higher loading rates [10]. Rate dependent tensile behavior in other high performance fiber reinforced cementitious composite has been observed and reported by others [11,12].

Deliberate engineering of tensile ductility of an impact resistant ECC under high rate loading is reported in this paper. What follows is a brief review of the theoretical foundation behind tensile strain-hardening response of ECC under dynamic loading. The experimental tensile stress–strain behavior of ECC mixes engineered based on insights gained from the theoretical considerations and micromechanical studies is then reported. Finally, low speed impact responses of ECC versus brittle concrete or mortar structural elements are compared.

2. Strain-hardening model for ECC under impact loading

The dynamic energy release rate for a crack propagating at velocity V is defined [13] as

$$G(\Gamma=)\lim_{\Gamma\to 0}\int_{\Gamma}\left(W+\frac{1}{2}\rho V^2\frac{\partial u_i}{\partial x}\frac{\partial u_i}{\partial x}\right)dy-\sigma_{ij}n_j\frac{\partial u_i}{\partial x}ds \tag{1}$$

where W is the strain energy density, ρ is the density, u_i is the displacement component, σ_{ij} is the stress component, and n_i is the unit normal vector. Eq. (1) is in general not path independent except for the special case when the crack propagates in a steady-state mode. For a steady-state crack propagating against a matrix toughness of G_{tip} and crack face bridging traction $\sigma_B(\delta)$ under remote steady-state tensile stress σ_{ss} and steady-state crack opening δ_{ss}, it can be shown [10] that

$$G_{tip}=\sigma_{ss}\delta_{ss}-\int_0^{\delta_{ss}}\sigma_B(\delta)d\delta\equiv G'_b \tag{2}$$

using the close contour in Fig. 4.

This is the same result as for the quasi-static loading case for which V = 0 [14]. This can be expected since the additional kinetic energy term involving V in Eq. (1) is a product with $(\partial u_i/\partial x)dy$. For the horizontal contour dy = 0 while for the vertical contours the $(\partial u_i/\partial x)$ term is uniformly zero given the steady-state crack propagating (in the x-direction) condition. Thus the required balance between matrix toughness G_{tip} and the complimentary energy G_b' is also identical to the quasi-static case. Specifically, since G_b' is limited by its maximum value attained when $\sigma_{ss}=\sigma_0$ when $\delta_{ss}=\delta_0$, the condition for steady-state flat crack propagation mode under dynamic or static condition can be stated as

$$G_{tip}<\sigma_0\delta_0-\int_0^{\delta_{ss}}\sigma_B(\delta)d\delta\equiv C \tag{3}$$

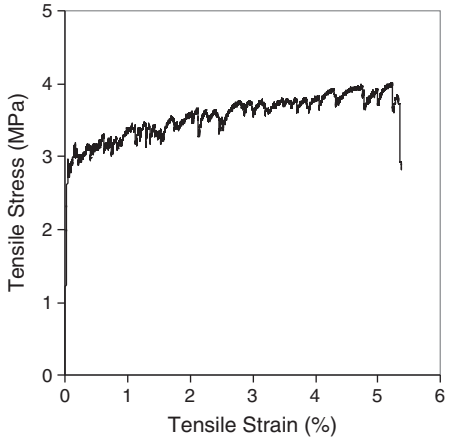

Fig. 2. Typical ECC tensile stress–strain curve (specimen size is 304.8 mm × 76.2 mm × 12.7 mm, fiber length is 12 mm).

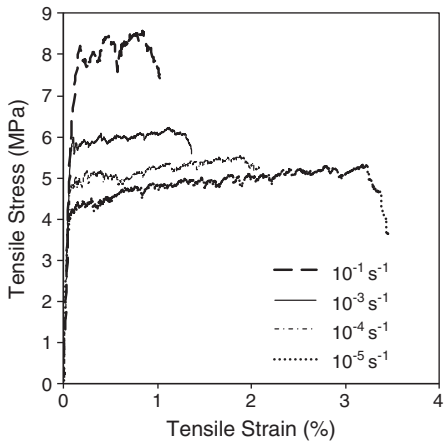

Fig. 3. Rate dependence in ECC M45 tensile stress–strain curve.

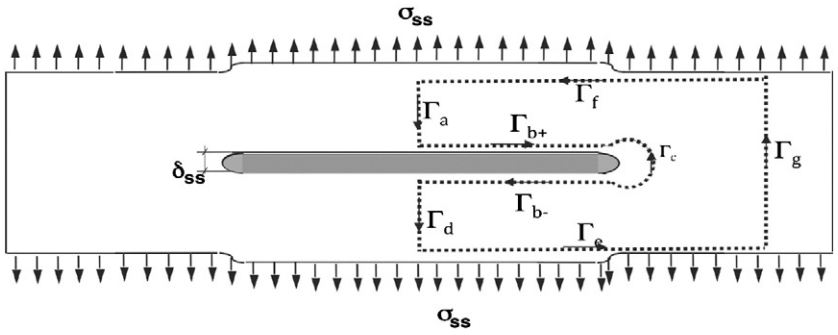

Fig. 4. A contour path for dynamic energy release rate calculation.

where C is the maximum complimentary energy as defined above. In other words, the engineering of fiber reinforced composites for flat crack propagation under dynamic loads follows exactly that under quasi-static loads, with the exception that the matrix toughness G_{tip} and the fiber bridging property $\sigma_B(\delta)$ may now be loading rate sensitive. Rate sensitivity of $\sigma_B(\delta)$ may result from the rate sensitivity of the reinforcing fiber or the fiber/matrix interface [15]. This may in turn result in a change in G_{tip} and C causing a violation of the inequality sign in Eq. (3) at higher loading rates, even when this inequality is satisfied under quasi-static loading condition.

Another condition for the pseudo strain-hardening is that the matrix first cracking strength σ_{fc} must not exceed the maximum fiber bridging strength σ_0.

$$\sigma_{fc} < \sigma_0 \tag{4}$$

where σ_{fc} is determined by the matrix toughness, the pre-existing internal flaw size, and crack face bridging traction $\sigma_B(\delta)$ and σ_0 is determined from $\sigma_B(\delta)$. Again, the matrix toughness and the $\sigma_B(\delta)$ can be loading rate sensitive. This may in turn result in a change in σ_{fc} and σ_0 causing a violation of the inequality sign in Eq. (4) under higher loading rates even when this inequality is satisfied under quasi-static loading condition.

Satisfaction of both Eqs. (3) and (4) is necessary to achieve ductile strain-hardening behavior. A material that exhibits ductile response under quasi-static loading may respond in a brittle manner under dynamic loading, due to material rate sensitivity in fiber, matrix and fiber/matrix properties as reflected in rate-dependent $\sigma_B(\delta)$ and G_{tip}. Details of the dynamic strain-hardening model and micromechanical characterization at high loading rates can be found in Ref. [9]. By testing for fiber, matrix and interface properties at loading speed from 0.001 mm/s to 10 mm/s, it was observed that the ratio C/G_{tip} of ECC M45 dropped by a factor of 2 and the ratio σ_0/σ_{fc} of M45 reduced by 10% under dynamic loading rate compared with those at quasi-static loading rate, resulting in loss of tensile ductility under impact loading as indicated in Fig. 3.

3. ECC engineered for impact resistance

Eqs. (3) and (4) provide insights for the design of ductile ECC resilient to dynamic loading. Specifically, given the sensitivity of the fiber/matrix interface toughness to loading rate, fibers with a hydrophobic surface may be deliberately chosen to eliminate the fiber/matrix chemical bond strength, so that only the rate insensitive frictional bond is present. Alternatively, the interfacial transition zone between the fiber and the bulk matrix may be modified to lower the amount of hydration products that chemically binds the fiber to the matrix. One such approach was to increase the pozzolanic fly ash content in the binder. Fly ash is known to reduce chemical bonding while increasing frictional bonding of the PVA fiber/matrix interface [16] favorable to inducing steady-state cracking. In addition, fly ash replacement of cement is also known to lower the matrix toughness. Thus a fiber with a hydrophobic surface and/or a matrix with higher fly ash content can be used to compensate the rate sensitivity of the material components that limits the tensile ductility at higher loading rates.

To explore the above material ingredient tailoring ideas suggested by the dynamic micromechanical model, two impact resistant ECC mixes (B and C) were prepared for testing. Their ingredient proportions are shown in Table 1. A control mix A was included. The cement used was Type I Portland Cement from Holcim Cement Co., MI, USA. The water reducing agent used was ADVA Cast 530 from W. R. Grace & Co., IL, USA. Two types of discontinuous polymer fibers, K-II REC™ polyvinyl alcohol (PVA) fiber from Kuraray Co. Ltd of Osaka, Japan, and Spectra 900 high strength high modulus polyethylene (PE) fiber from Honeywell Inc., USA, were used at 2% volume fraction. The properties of the PVA and PE fibers are shown in Table 2. The pozzolanic admixture used was a low calcium Class F fly ash from Boral, TX, USA. The F110 silica sand with a size distribution from 50 to 250 μm, from US Silica Co., MV, USA, was used.

Control mix A represents a PVA-ECC (ECC M45) that has established tensile ductility under quasi-static loading, but experienced a drastic loss of ductility under higher rate loading as shown in Fig. 3. Mix B (HFA-ECC) more than doubles the fly ash content compared to the control mix. The water content is also increased in order to maintain the same water/binder ratio of 0.26. This retailoring leads to a reduction in both fiber/matrix interfacial chemical bond and matrix toughness [10]. Mix C (PE-ECC) replaces the hydrophilic PVA fiber by a hydrophobic high modulus polyethylene (PE) spectra fiber, thus completing eliminating the interfacial chemical bond. These measures lead to a larger margin of C/G_{tip}, favoring tensile ductility.

A uniaxial tensile test was conducted to characterize the tensile behavior of the composites. The coupon specimen used here measures 304.8 mm × 76.2 mm × 12.7 mm. Tests were conducted in an MTS machine with 25 KN capacity under displacement control. The

Table 1
Mix proportions of examples, parts by weight.

Mix no.	Cement	Water	Sand	Fly ash	SP	PE fiber by volume	PVA fiber by volume
A	1	0.58	0.8	1.2	0.012	0	0.02
B	1	1	1.4	2.8	0.013	0	0.02
C	1	0.68	0	1.6	0.013	0.02	0

Table 2
Properties of KII-REC PVA and Spectra 900 PE fibers.

Fiber type	Nominal strength (MPa)	Diameter (μm)	Length (mm)	Initial tangent modulus of elasticity (GPa)
PVA	1620	39	12	42.8
PE	2400	38	38	66

Table 3
Measured properties of example mixes.

Mix no.	Mix name	Tensile strength (MPa)		Tensile strain capacity (%)		Compressive strength (MPa)
		Strain rate (s^{-1})				Quasi-static
		10^{-5} (quasi-static)	10^{-1}	10^{-5} (quasi-static)	10^{-1}	
A	ECC M45	5.3	8.6	3.2	0.8	53
B	HFA-ECC	4.8	5.9	3.7	3.8	40
C	PE-ECC	2.3	4.2	3.0	3.2	48

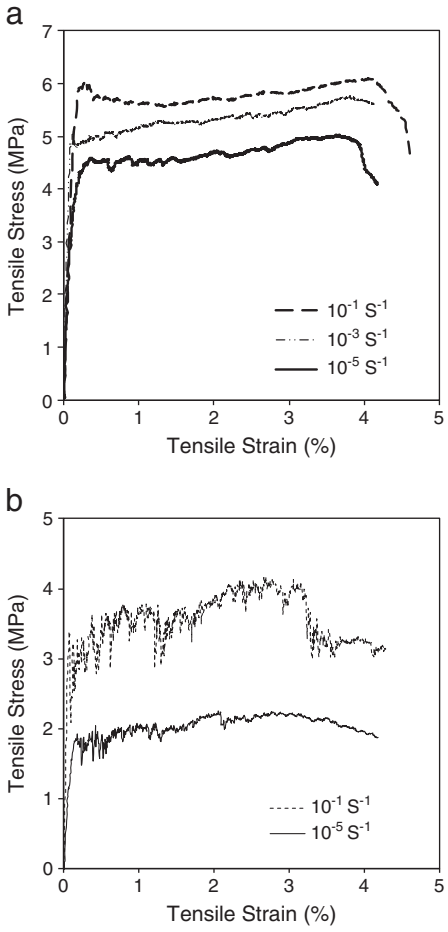

Fig. 5. Tensile stress–strain curves of (a) HFA-ECC (mix B) and (b) PE-ECC (mix C) at various strain rates, at 28 days of age.

test strain rate ranges from $10^{-5}\,s^{-1}$ to $10^{-1}\,s^{-1}$, corresponding to quasi-static loading to low speed impact. Two LVDTs with a gage length of 100 mm measured the deformation during load.

The test results are summarized in Table 3, including tensile strain capacity and strength at both the quasi-static and the highest test rate ($10^{-1}\,s^{-1}$), and compressive strength at quasi-static loading for each mix, at 28 days age. Complete tensile stress–strain curves of these composites are shown in Figs. 3 and 5. The retailored mixes (mixes B and C) exhibit significant strain-hardening behavior when subjected to strain rate ranges from $10^{-5}\,s^{-1}$ to $10^{-1}\,s^{-1}$. The results show a substantial increase in the ultimate tensile strength with increasing strain rate, while the strain capacity can be retained with similar multiple cracking behavior as those for the static test. Unlike mix A, the higher strain rates do not seem to negatively affect the strain-hardening behavior of these retailored ECCs.

4. Impact response of ECC panels

Fig. 6 shows an image sequence of the damage process of impact resistant ECC (mix B) in a drop weight test, using a high-speed camera. The drop mass (flat tup) and drop height were 12 kg and 0.5 m, respectively. The ECC square shaped panel measuring 305 mm × 305 mm × 25.4 mm (length × height × depth) rested on a steel frame support along its edges. No steel reinforcement was applied to this ECC panel. A maximum strain rate on the tension (distal) side is estimated to be in the range of $10^{0}\,s^{-1}$ to $10^{1}\,s^{-1}$. A puff of dust was observed at impact (Fig. 6a and b) by the loading tup. As the tup rebounded, no damage can be observed on the impact face (Fig. 6c). Examination of the distal side of the panel showed no damage either. Microcracks on this side were observed only after the test was performed three times.

For comparison, the same test was run on a similar size mortar specimen with 0.5% steel reinforcement. In this case, the loading tup penetrated the mortar panel on first impact (Fig. 7). Failure by brittle fracture occurred both around the tup (Fig. 7b,c) and at one of the corners (Fig. 7d) as the panel bent against the perimeter steel support.

5. Impact response of ECC and R/ECC beams

An ECC mix B beam measuring 305 mm × 76 mm × 51 mm (length × height × depth) and reinforced by a single steel bar was tested under three-point-bending drop weight impacts. The 5 mm diameter smooth steel bar was placed close to the bottom side with a clear cover of 18 mm. The reinforcing ratio was 0.5%. A control specimen using reinforced concrete ($f_c' = 40$ MPa) was also tested.

A 50 kg impact tup with flat impact surface was dropped freely from a height of 0.5 m onto the specimen center. A maximum strain rate at the bottom of the beam side is estimated to be in the range

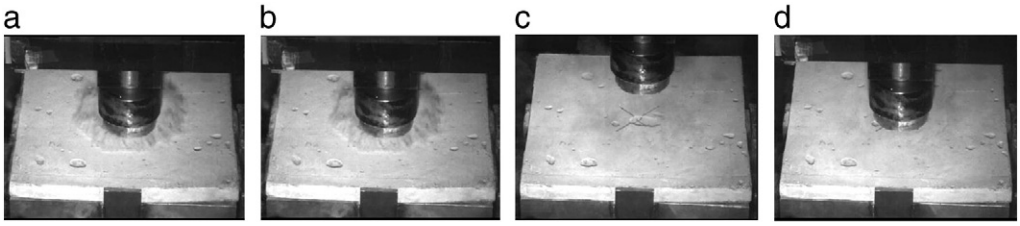

Fig. 6. High-speed camera image sequence captured at (a) impact, and (b) immediately after impact, (c) tup rebound and (d) tup impacted onto the ECC panel again.

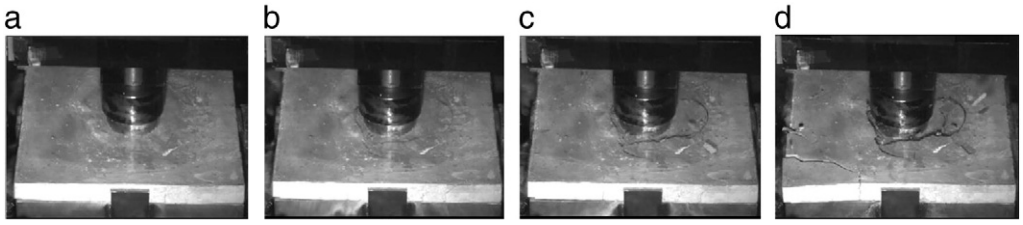

Fig. 7. High-speed camera image sequence captured (a) at impact, and (b–d) at three time instances immediately after impact.

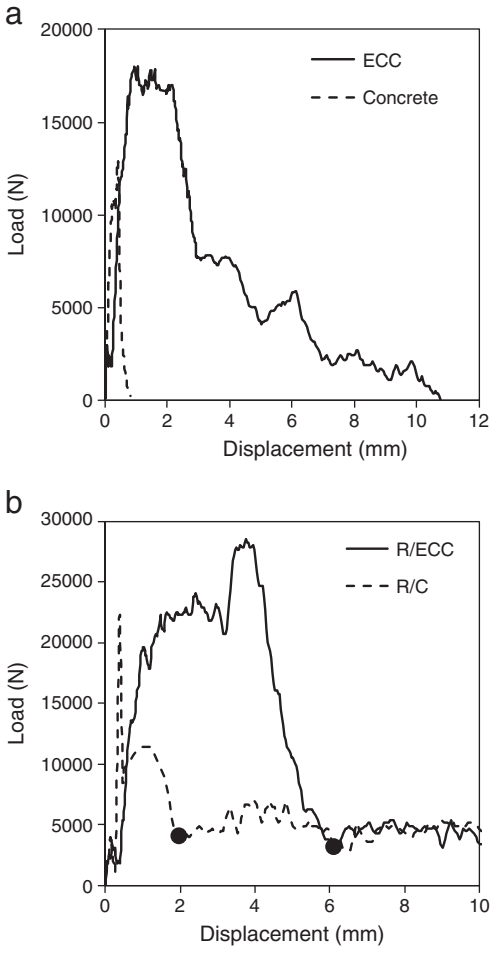

Fig. 8. Load–displacement relationships of (a) ECC and concrete beams, and (b) R/ECC and R/C beams in single impact experiment.

of $10^0\ s^{-1}$ to $10^1\ s^{-1}$. The mass and height were chosen so that the specimens failed in one single impact. The specimens were supported with a span of 254 mm. A steel roller was glued in the middle span and on the top surface of the specimens so that a uniform line load was applied to the specimen when the tup contacted the roller. 1 mm thick hard rubber pads were placed in between the specimen, the roller, and the tup.

Table 4
Load and energy capacity of concrete, R/C, ECC, and R/ECC beams in single impact experiment.

	Concrete	R/C	Improvement due to reinforcement	ECC	R/ECC	Improvement due to reinforcement
Load capacity (kN)	13	22	9	18	29	11
Energy capacity (N-m)	4	17	13	69	102	33

Fig. 8a shows the load–displacement curve of the concrete and ECC beams and Fig. 8b plots the load–displacement curve of the R/C and R/ECC beams. The energy dissipation of beams without reinforcement was the area below the load–displacement curve. For reinforced beams, the failure state was defined as when a plateau load capacity (~5 kN for both specimens, marked by the two solid dots) was reached on softening after peak load. At this stage, pullout of the steel reinforcing bar assumed after a crack completely penetrated through the depth of the specimen. Therefore, the energy capacity of R/C and R/ECC beams was computed as the area below the load–displacement curve until the solid dots.

Table 4 summarizes the load and energy capacities of the four beams. While the load capacity of the R/ECC beam was increased only by 32% from that of the R/C beam, from 22 kN to 29 kN, the energy capacity was increased by 500% (from 17 N-m to 102 N-m). Interestingly, the load capacity improvement due to the addition of steel reinforcing bar of the R/ECC was increased by 22%, from 9 kN to 11 kN. The energy capacity improvement due to the addition of the reinforcement of the R/ECC was increased by 150%, from 13 N-m to 33 N-m. This implies that the addition of steel reinforcing bars for enhancing structural load and energy capacities is more efficient in R/ECC than that in R/C. This is likely due to the high tensile ductility of ECC so that a compatible deformation between steel reinforcement and ECC was achieved during impact, engaging a longer segment of steel to undergo plastic yielding. Synergistic interaction between reinforcing steel and ECC was also observed in other R/ECC elements subjected to quasi-static loading [17].

To evaluate the resistance of R/C and R/ECC beams under multiple impacts, the same test configuration was adopted except that a 12 kg impact tup was chosen and the drop height was reduced to 0.2 m. Again, the R/ECC beams showed much improved impact resistance over that of R/C beams. Fig. 9 summarizes the load capacity of R/C and R/ECC beams in each impact. It was found that the R/C beam failed after the first impact at about 9 kN (the data point showing load capacity ~5 kN at the 2nd impact is due to the pullout of reinforcing bar). However, the load capacity of R/ECC remains roughly constant at about 20 kN over the ten impacts. Fig. 10 shows the damage of R/C

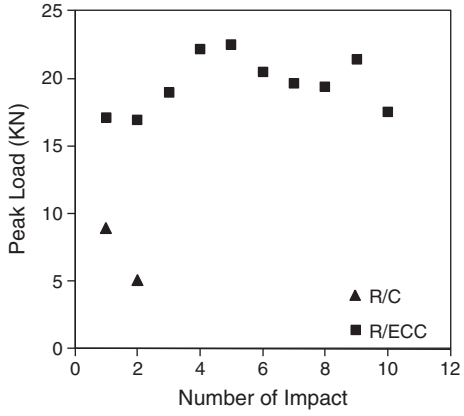

Fig. 9. Peak load recorded in multiple impacts.

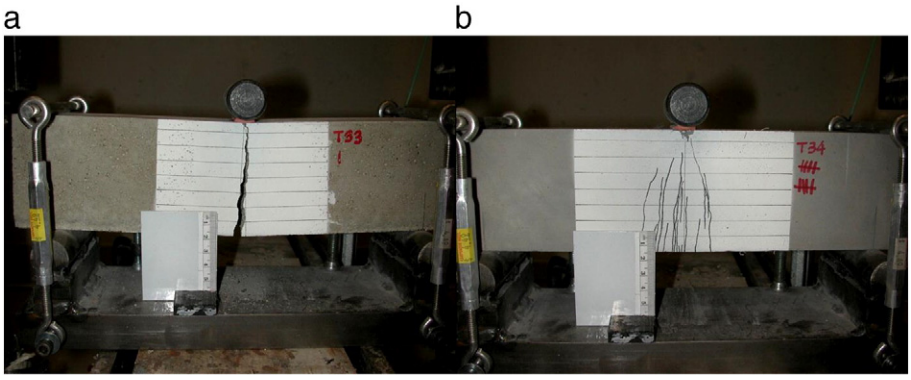

Fig. 10. Damage of (a) R/C beam after the 1st impact (cracking penetrated through specimen) and (b) R/ECC beam after the 10th impact (fine cracks only highlighted by a thick marker).

and R/ECC after impact testing. As can be seen, one single crack with large crack width appeared in the R/C beam after the first impact. The crack penetrated through the beam causing severe loss of structural integrity and load carrying capacity. In contrast, only very fine microcracks were found in R/ECC specimen even after 10 impacts. This experiment demonstrates the potential for R/ECC elements to sustain multiple impact loads while maintaining damage tolerance.

6. Discussions and conclusions

The improvement of damage tolerance and energy dissipation in concrete material is important for enhancing resiliency of civil infrastructure against multi-hazards such as earthquake, projectile impact and bomb blasts. The impact response of concrete has been widely studied in the last several decades. These studies generally point to the rate sensitivity of concrete that shows a higher strength accompanied by a higher brittleness as the loading rate increases. Previous studies of ECC under increasing loading rate also point to the same phenomena.

In the present study, the intrinsic material source of rate sensitivity in ECC material was identified via dynamic steady-state crack propagation analyses. The fracture and micromechanical analyses provide insights into specific selection of fiber, matrix ingredient and fiber/matrix interface control to maintain tensile ductility under dynamic loading. By deliberate adjustment of the micromechanical parameters that governs rate sensitivity, two impact resistant ECC mixes, one containing hydrophobic fiber and the other containing a high dosage of fly ash, were designed and demonstrated tensile strain capacity in excess of 3% at all strain rates spanning fours orders of magnitude from 10^{-5} s^{-1} to 10^{-1} s^{-1}. It is concluded that the ingredients of ECC can be systematically tailored to maintain high impact resistance, using insights from the strain-hardening model for ECC under dynamic loading as guidance.

Drop weight tower tests on panels and beams confirmed that the material ductility of impact resistant ECC transformed into enhancements of load and energy dissipation of these structural elements. Damage on the impact resistant ECC retained the multiple microcracking characteristics commonly observed in quasi-static loading of regular ECC, thus delaying the localization of a single fracture and allowing the engagement of a longer segment of steel to undergo plastic yielding and energy absorption. It is concluded that the ductility of the redesigned ECC for dynamic loading carries over into damage tolerant structural response.

The material and small structural element studies reported in this paper confirm the concept that concrete material can be tailored for resilient infrastructure under impact. These experiments also validate the effectiveness of the use of the dynamic steady state crack analyses and strain hardening criteria for material design for ductility under dynamic loading. However these experimental studies were conducted on limited specimen sizes and loading rates. Further studies employing more realistic size specimens, loading type and still higher loading rates associated with high velocity impact or blast are necessary to demonstrate the full effectiveness of ductile ECC for infrastructure protection.

Acknowledgments

The drop weight impact test on ECC panels was conducted by Dr. Mo Li and Mr. Amit Salvi. Image capture was conducted in the Composite Structures Laboratory directed by Prof. A. Waas. Partial support of this research by the National Science Foundation and by the University of Michigan is gratefully acknowledged.

References

[1] J. Shinozuka, T. Obikawa, High Levels of Hydrostatic Stress at Shear Zone Induced by Plastic Shock Waves under Ultra High-speed Cutting Conditions, Proceedings of the 10th CIRP International Workshop on Modeling of Machining Operations, August 27–28, 2007, Reggio Calabria, Italy, ed. Fabrizio Micari and Luigino Filice, 2007, pp.357–364.
[2] L.J. Malvar, C.A. Ross, Review of strain rate effects for concrete in tension, ACI Mater. J. 95 (6) (1998) 735–739.
[3] G. Fischer, V.C. Li (Eds.), International RILEM Workshop on High Performance Fiber Reinforced Cementitious Composites in Structural Applications, RILEM Publications SARL, 2006.
[4] K. Rokugo, T. Kanda, H. Yokota, N. Sakata, Applications and recommendations of high performance fiber reinforced cement composites with multiple fine cracking (HPFRCC) in Japan, Mater. Struct. 42 (2009) 1197–1208.
[5] V.C. Li, On engineered cementitious composites (ECC) — a review of the material and its applications, J. Adv. Concr. Technol. 1 (3) (2003) 215–230.
[6] E. Yang, V.C. Li, Strain-hardening fiber cement optimization and component tailoring by means of a micromechanical model, Construct. Build Mater. 24 (2) (2010) 130–139.
[7] G. Fischer, V.C. Li, Influence of matrix ductility on the tension-stiffening behavior of steel reinforced engineered cementitious composites (ECC), ACI Struct. J. 99 (1) (2002) 104–111.
[8] G. Fischer, Deformation behavior of reinforced ECC flexural members under reversed cyclic loading conditions, Ph.D. Dissertation, Civil and Environmental Engineering, University of Michigan, 2002.
[9] E.H. Yang, V.C. Li, Rate dependence in engineered cementitious composites, Proceedings, HPFRCC-2005 International Workshop. Honolulu, Hawaii, USA, 2005.
[10] E.H. Yang, Designing Added Functions in Engineered Cementitious Composites, PhD Dissertation, Department of Civil and Environmental Engineering, University of Michigan, 2007.
[11] V. Mechtcherine, O. Millon, M. Butler, Behaviour of SHCC under impact loading, Cem. Concr. Compos. 22 (2011) 1–11.
[12] J.K. Dong, S. El-Tawil, A.E. Naaman, Rate-dependent tensile behavior of high performance fiber reinforced cementitious composites, Mater. Struct. 42 (3) (2009) 399–414.
[13] L.B. Freund, Dynamic Fracture Mechanics, Cambridge University Press, Cambridge, New York, 1990.
[14] D.B. Marshall, B.N. Cox, A J-integral method for calculating steady-state matrix cracking stresses in composites, Mech. Mater. 8 (1988) 127–133.
[15] W.P. Boshoff, V. Mechtcherine, G. van Zijl, Characterizing the time-dependant behaviour on the single fibre level of SHCC: part 2: the rate effects on fibre pull-out tests, Cem. Concr. Res. 39 (2009) 787–797.
[16] E. Yang, Y. Yang, V.C. Li, Use of high volumes of fly ash to improve ECC mechanical properties and material greenness, ACI Mater. J. 104 (6) (2007) 620–628.
[17] G. Fischer, V.C. Li, Influence of matrix ductility on the tension-stiffening behavior of steel reinforced engineered cementitious composites (ECC), ACI Struct. J. 99 (1) (2002) 104–111.